# Phase Noise Analysis of Resonator-Enhanced Electro-Optic Comb-Based Analog Coherent Receivers

Elizabeth Chen, *Student Member, IEEE*, Brandon Buscaino, *Member, IEEE*, and Joseph M. Kahn, *Fellow, IEEE*

***Abstract*—We present an architecture for wavelength-division-multiplexed coherent data center links employing resonator-enhanced electro-optic frequency comb generators as both transmitter and local oscillator (LO) sources. We show that in each frequency comb, the phase noise in all comb lines is determined completely by the optical phase noise of the seed laser and the phase noise of the microwave oscillator. We propose an analog coherent receiver that performs carrier recovery on all wavelength channels using only two phase-locked loops. We use an independent cascade of phase shifters driven by marker tone detection in each channel for polarization recovery and compensation of a static optical phase shift. We study design examples for quadrature phase-shift keying and 16-ary quadrature amplitude modulation (16-QAM), determining requirements on the transmitter and LO seed laser linewidths and the LO frequency modulation (FM) response. We find that for a dual-polarization (DP) 16-QAM link with 17 wavelength channels, each operating at 56 GBaud, if the combined linewidth of the transmitter and LO seed lasers is 100 kHz, the LO seed laser requires an FM response that is flat from d.c. to several hundred MHz to maintain a phase-error penalty below 1 dB.**

***Index Terms*—Carrier phase recovery, coherent detection, data centers, optical frequency comb, optical phase-locked loop.**

## I. Introduction

COHERENT detection provides a promising option for future data center optical links. It allows data rates per channel to be increased using modulation formats such as dual-polarization (DP) phase-shift keying (PSK) or quadrature-amplitude modulation (QAM) [1]. Moreover, mixing a received signal with a strong local oscillator (LO) improves receiver sensitivity [2], helping support higher data rates and overcoming losses in advanced network architectures and highly integrated transceiver subsystems [3].

Long-haul optical communication systems prioritize reach, and therefore implement potentially power-hungry coherent receivers that extensively use digital signal processing (DSP). Data center links, by contrast, are highly cost- and power-constrained, and may employ digital or analog coherent receivers that sacrifice reach and tolerance to transmission impairments to reduce cost and power consumption.

To address demands for low-power data center links, various combinations of optical and electronic analog techniques for polarization and carrier recovery (CR) have been studied. The coherent receiver in [4] achieves both polarization demultiplexing and CR using analog multipliers. The single-wavelength DSP-free coherent receiver in [5] performs polarization derotation using cascaded optical phase shifters and CR using optical or electrical phase-locked loops (PLLs). A design using phase shifter-based polarization recovery and using a single laser for both the transmitter and LO, obviating the need for CR, has been demonstrated in [6]. Analog coherent receivers retaining chromatic dispersion compensation capability using analog adaptive equalizers have also been proposed [7].

Optical frequency combs are promising sources for data center systems, potentially reducing the cost and power consumption per wavelength-division-multiplexed (WDM) channel [8]. The phase noise coherence across comb lines can simplify CR at a coherent receiver [9]. DSP-based joint CR of multiple WDM channels has been considered [10]. Phase locking transmitter and LO combs using analog techniques is attractive from a power efficiency standpoint. Experiments have demonstrated that transmitter and LO combs can be phase-synchronized by transmitting a marker tone to injection lock the LO comb seed laser [11]. An analog CR scheme that regenerates the LO comb by using optical injection locking and an electrical PLL with two marker tones can obviate the need for DSP-based CR in a coherent receiver [12].

In scaling low-power analog coherent receivers to WDM systems, one approach is to perform CR independently for each channel [13]. In this paper, we study a WDM system architecture combining analog coherent receivers with frequency combs to dramatically simplify CR. Both transmitter and LO sources are dual-ring resonator-enhanced electro-optic (DR-EO) comb generators, which can be fabricated using integrated passive optical elements and offer high power conversion efficiency [14]. CR for WDM channels is performed using only two optical PLLs (OPLLs). Polarization de-multiplexing and removal of constant phase offsets between signal and LO are performed using optical

Manuscript received 4 April 2022; revised 5 July 2022 and 16 August 2022; accepted 18 August 2022. Date of publication 22 August 2022; date of current version 4 November 2022. This work was supported by Maxim Integrated (now Analog Devices, Inc.) and Inphi Corporation (now Marvell). *(Corresponding author: Elizabeth Chen.)*

The authors are with the Department of Electrical Engineering, Stanford University Ginzton Laboratory, Stanford, CA 94305 USA (e-mail: echen105@stanford.edu; buscaino@alumni.stanford.edu; jmk@ee.stanford.edu).

Color versions of one or more figures in this article are available at https://doi.org/10.1109/JLT.2022.3200632.

Digital Object Identifier 10.1109/JLT.2022.3200632

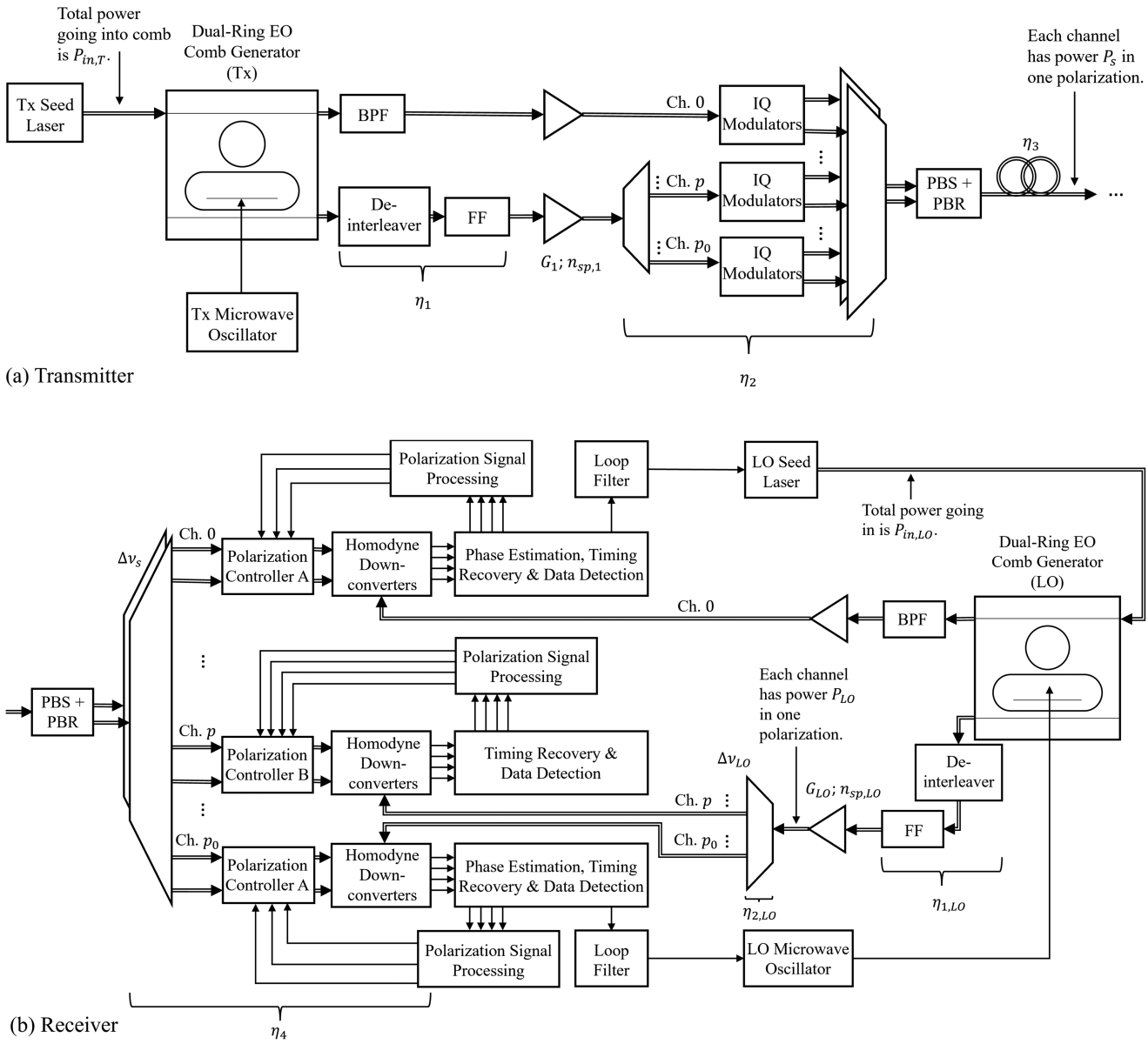


Fig. 1. (a) Transmitter and (b) receiver of the proposed frequency comb-based multi-wavelength analog coherent link architecture. The transmitter and receiver use independent DR-EO comb generators as their optical sources. The receiver uses OPLLs on channels 0 and $p_0$ to perform CR and uses phase-shifter-based polarization controllers of type A or B for polarization de-multiplexing and/or removing constant phase offsets on all channels. The $\eta_i$ denote optical losses, while the $G_i$ and $n_{sp,i}$ denote amplifier gains and spontaneous emission factors. BPF: bandpass filter, Ch.: channel, FF: flattening filter, IQ: in-phase and quadrature, PBS/R: polarization beam splitter/rotator.

phase shifters controlled by low-speed marker tone detection circuitry. We focus on analyzing the phase noise performance of this system and show that the architecture is suitable for DP quadrature phase-shift keying (DP-QPSK) and DP-16-QAM modulation formats.

The remainder of this paper is organized as follows. In Section II, we describe the DR-EO comb-based analog coherent receiver architecture and study how it performs key functions. In Section III, we analyze how the DR-EO comb generator affects phase noises from optical and microwave sources, which is crucial for modeling CR performance. In Section IV, we study how phase noise affects comb-based link design examples and also discuss effects of other signal distortion sources. We conclude the paper in Section V.

## II. Architecture Overview

The proposed multi-wavelength analog coherent link architecture is shown in Fig. 1. DR-EO comb generators are used as both transmitter and LO sources. Before data is modulated onto separate comb lines at the transmitter, the comb undergoes pre-processing operations by a de-interleaver (DI), flattening filter (FF), bandpass filter (BPF) and semiconductor optical amplifiers (SOAs), as required. The DI ensures a sufficiently large channel spacing when the comb spacing is too small

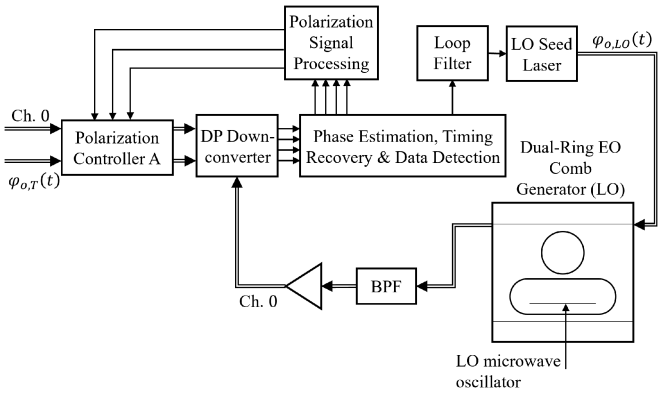


Fig. 2. Central channel (Ch. 0) of the comb-based WDM analog coherent receiver. Polarization controller type A performs polarization recovery, while an OPLL controlling the phase of the LO comb seed laser compensates phase noise from the transmitter and LO comb seed lasers.

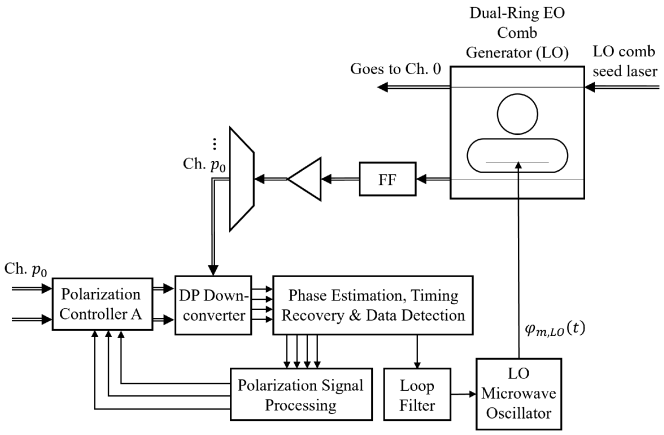


Fig. 3. Outer reference channel (Ch. $p_0$) of the comb-based WDM analog coherent receiver. Polarization controller type A performs polarization recovery, while an OPLL controlling the phase of the LO comb microwave oscillator compensates phase noise from the transmitter and LO comb microwave oscillators.

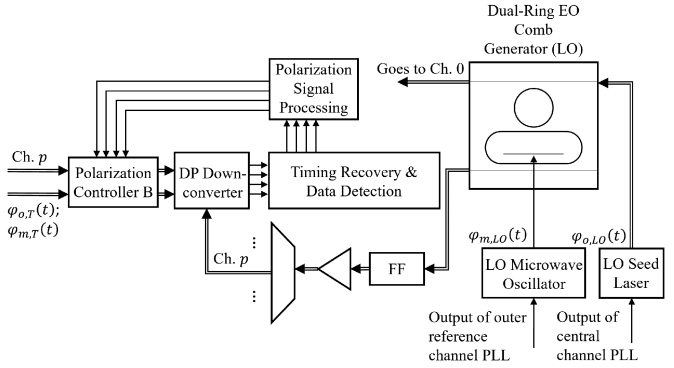


Fig. 4. Remaining channels (Ch. $p$) of the comb-based WDM analog coherent receiver. In each channel, a polarization controller type B performs polarization recovery and removal of a constant phase offset. No additional phase-tracking mechanism is used for these channels.

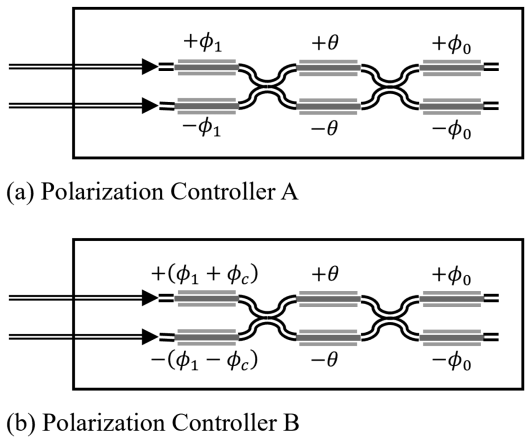


Fig. 5. Polarization controllers (a) type A and (b) type B. Controller type A compensates for polarization rotation using three phase shifters driven by three low-speed control signals. Controller type B compensates for polarization rotation and an additional constant phase offset using three phase shifters driven by four low-speed control signals.

to accommodate for the symbol rate. Similar pre-processing operations are performed on the LO comb at the receiver. Fig. 1 is drawn assuming an intra-data center link operating in the O-band. An inter-data center link operating in the C-band might also include erbium-doped fiber amplifiers inline with the fiber link (these are not shown in Fig. 1).

At the receiver, channels modulated onto different comb lines are subject to different signal processing operations. We identify three categories of channels, which are denoted by their comb line indices: (1) the central channel 0, (2) an outer reference channel $p_0$, and (3) the remaining channels, each denoted by an arbitrary index $p$. These are labeled as Ch. 0, Ch. $p_0$ and Ch. $p$ in Fig. 1. The central channel employs a PLL controlling the LO comb seed laser. The outer reference channel employs another PLL controlling the LO comb microwave oscillator. The remaining channels do not employ feedback loops affecting the LO comb.

The central channel (see Fig. 2) and outer reference channel (see Fig. 3) perform polarization de-multiplexing using polarization controllers of type A (see Fig. 5(a)), similar to the DSP-free coherent receiver in [5]. These channels perform CR using OPLLs. The polarization controllers and OPLLs are described in detail in the following sections.

In contrast to the central and outer reference channels, the remaining channels (see Fig. 4) do not need to employ OPLLs for CR. These channels use polarization controllers of type B (see Fig. 5(b)) to perform polarization de-rotation and removal of constant phase offsets.

### A. Polarization Demultiplexing

Polarization rotation typically varies on a timescale of several milliseconds in short-reach links [15], and can be compensated by an optical polarization controller driven by low-speed circuitry. The polarization controller type A used on the central and outer reference channels is shown in Fig. 5(a).

In order to recover polarization, the transmitter sends a low-frequency marker tone on the X-polarization of the in-phase (I) component (the XI tributary). After reaching the receiver, the marker tones detected on the XQ, YI and YQ tributaries are

extracted using low-pass filters (LPFs) and passed to a microcontroller, which adjusts the three phase shifters of polarization controller type A to minimize the marker tones detected in the latter three tributaries. This polarization recovery scheme is discussed in [5].

The proposed polarization controller can be implemented using thermo-optic phase shifters, which have low losses and response times on the order of several microseconds to several tens of microseconds [16], potentially enabling a low-cost and low-power solution [13]. Endless polarization control can be accomplished by resetting the phase shifters when they are close to their excursion limits, using interleaving to compensate for the associated burst errors [5].

### B. Phase Offset Removal

Channels other than the central and outer reference channels do not employ OPLLs for carrier synchronization (see Fig. 4), since only a constant phase offset between the signal and LO needs to be removed. Both polarization de-rotation and removal of the constant phase offset can be accomplished using polarization controller type B shown in Fig. 5(b). Controller type B has four controlled phases $(\phi_1, \phi_c, \theta, \phi_0)$. We describe the polarization and phase offset recovery scheme in this section.

We can define a unitary matrix $T_{ch}$ describing polarization transformation and an overall phase offset. The matrix describing polarization controller type B in Fig. 5(b) is

$$T_{cont} = \begin{bmatrix} e^{\phi_0} & 0 \\ 0 & e^{-j\phi_0} \end{bmatrix} \cdot \begin{bmatrix} \cos(\theta) & -j\sin(\theta) \\ -j\sin(\theta) & \cos(\theta) \end{bmatrix} \cdot \times \begin{bmatrix} e^{j(\phi_1+\phi_c)} & 0 \\ 0 & e^{-j(\phi_1-\phi_c)} \end{bmatrix}. \quad (1)$$

In order to compensate for the polarization rotation and constant phase offset, marker tones at two different low frequencies are added to the drive signals of two different tributaries at the transmitter, modulating their amplitudes. Tone A is added to the XI tributary and tone B is added to the YI tributary. The phase shifters are adjusted by a microcontroller to minimize tone A's presence in the XQ, YI, and YQ tributaries and tone B's presence in the XI, XQ, and YQ tributaries. Fig. 6 shows the convergence of the bit-error ratio (BER) as the phase shifters are adjusted by the microcontroller. In this simulation, larger marker tone amplitudes and phase adjustment step sizes are used initially to facilitate faster convergence. The stronger marker tones cause a horizontal spread in the signal constellations, as seen in Fig. 6(b). The marker tone amplitudes and phase adjustment step sizes are then reduced around iteration 100, yielding a cleaner constellation, as in Fig. 6(c). This method results in a $180^\circ$ phase ambiguity in both polarizations, which can be resolved by including known training sequences in transmitted data or by using information obtained in error-correction decoding.

Fig. 7 shows the BER as a function of the SNR per symbol for 16-QAM when $T_{ch}$ is known and polarization rotation and phase offset are perfectly compensated. Fig. 7 also shows the BER vs. SNR when the phase shifters in polarization controller type B are adjusted using the marker tone detection scheme.

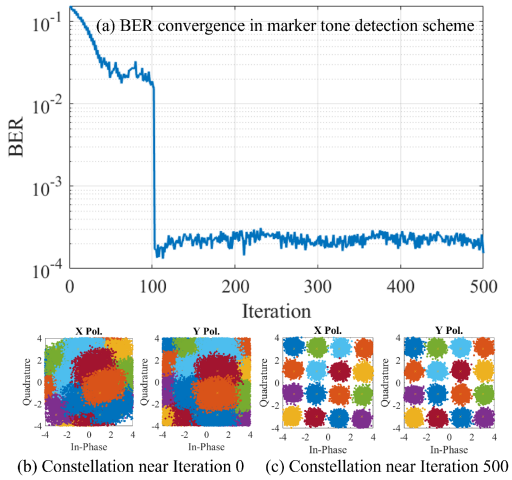


Fig. 6. (a) Convergence of the BER in the marker tone detection scheme. When the BER is high, the marker tone amplitude and phase adjustment increment are high, causing the constellation to spread, as in (b). When the BER is low, the marker tone amplitude and phase adjustment increment are small, resulting in a cleaner constellation, as in (c).

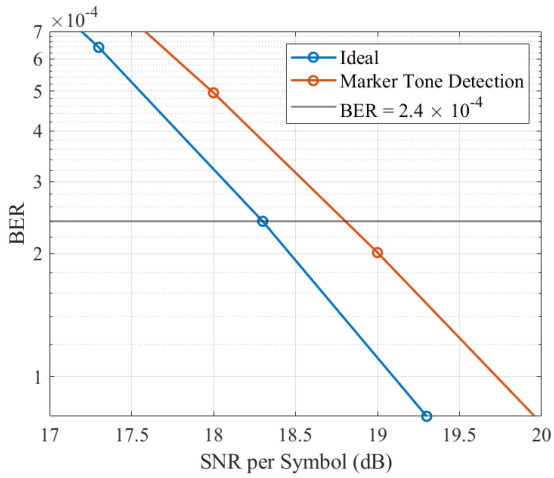


Fig. 7. BER versus SNR per symbol for 16-QAM when polarization rotation and phase offset are perfectly compensated (blue) or compensated by the marker tone detection scheme (red). Non-ideal compensation causes a 0.5-dB SNR penalty at a target BER of $2.4 \times 10^{-4}$.

At a target BER of $2.4 \times 10^{-4}$, marker tone detection results in an SNR penalty of about 0.5 dB.

Common polarization de-rotation for all channels is also possible. In this case, two cascaded phase shifters will be placed in front of the de-multiplexer in Fig. 1(b) for polarization de-rotation and an additional phase shifter for each channel will be placed after the de-multiplexer for phase offset cancellation. Common polarization control will, however, place substantial restrictions on link distance and total system bandwidth.

### C. Carrier Recovery

On the central and outer reference channels, CR is performed using OPLLs at the receiver. Each OPLL includes three key

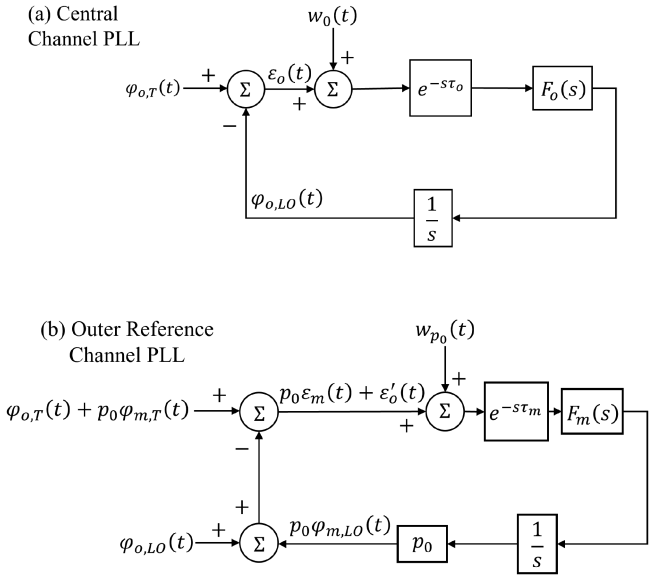


Fig. 8. Linearized models of (a) central channel OPLL. (b) Outer reference channel OPLL.

components: a phase estimator, a loop filter and a frequency-controllable oscillator. For the central channel, the oscillator is the seed laser for the LO DR-EO comb generator. For the outer reference channel, the oscillator is the microwave source driving the phase modulator in the LO DR-EO comb generator. To accommodate either QPSK or higher-order QAM, we can use analog or discrete-time decision-directed phase detection, which estimate phase error by taking the product of a decision on the complex signal and a delayed or sampled-and-held value of the signal [17], [18]. In this study, we consider a second-order loop filter described by a transfer function

$$F(s) = 2\zeta\omega_n + \frac{\omega_n^2}{s}. \tag{2}$$

In (2), $\zeta$ is the damping coefficient, commonly chosen to be $1/\sqrt{2}$, and $\omega_n$ is the loop natural frequency, which needs to be optimized to minimize the phase-error variance between the signal and LO. We denote the central channel and outer reference channel loop filters by $F_o(s)$ and $F_m(s)$, which have natural frequencies $\omega_{n,o}$ and $\omega_{n,m}$, respectively.[1]

Both the central channel and outer reference channel OPLLs can be studied using linearized models [18], which are shown in Figs. 8(a) and 8(b), respectively. These models take into account the effects of the DR-EO comb generator in the loop path, which are described in detail in Section III. The models in Figs. 8(a) and 8(b) use the following notation:

1) $\varphi_{o,T}(t)$ is the phase noise of the transmitter comb seed laser. $\varphi_{o,LO}(t)$ includes the phase noise of the LO comb seed laser as well as its control phase. We will refer to phase noise processes associated with the seed lasers as *optical phase noise*.
2) The phase error on the central channel is $\varepsilon_o(t)$. The phase difference between the transmitter and LO comb microwave modulation sources is denoted by $\varepsilon_m(t)$. The phase error arising from the comb microwave modulation sources on the outer reference channel is then $p_0\varepsilon_m(t)$. We refer to the phase difference between the transmitter and LO comb seed lasers as the *optical phase error* and that between the transmitter and LO comb microwave modulation sources as the *microwave phase error*.
3) $\tau_o$ and $\tau_m$ are the time delays arising from signal propagation and component group delays in the central channel and outer reference channel OPLLs, respectively.
4) $w_0(t)$ and $w_{p_0}(t)$ capture the effects of additive white Gaussian noise (AWGN) on the central and outer reference channels, respectively, including thermal, shot, and LO-signal spontaneous beat noises (see Appendix C). They have two-sided power spectral densities (PSDs) given by

$$S_{w_i w_i}(\omega) = \frac{\eta_c T_s}{2\gamma_i} \quad \text{for } i \in \{0, p_0\}, \tag{3}$$

where $\eta_c$ is a penalty factor associated with the transmitted constellation [18], $\gamma_0$ and $\gamma_{p_0}$ are the signal-to-noise ratios (SNRs) per symbol on the central and outer reference channels, respectively, and $T_s$ is the symbol interval [1].

## III. Effects of Resonator-Enhanced Electro-Optic Comb Generator

Using EO comb generators as the transmitter and LO light sources obviates the need for multiple discrete lasers and enables the simplified CR scheme described in Section II, since the phase noises on different comb lines are related. Phase noise characteristics of phase- and intensity-modulated EO combs have been studied theoretically and analytically [19]. However, the effects of resonators in the resonator-enhanced (RE) EO comb generator on phase noise is unclear. This section addresses how the optical and microwave phase noises of the seed laser and microwave modulation source are affected by the RE-EO comb generator.

Fig. 9 presents a single-ring electro-optic (SR-EO) comb generator. For the SR-EO comb generator shown, $k$ and $\gamma$ are the coupler power transmission and power insertion losses, respectively. $T$ is the round-trip time of the ring resonator and $(1-\alpha)$ is its round-trip loss. The cumulative round-trip amplitude gain can be defined as $r = \sqrt{\alpha(1-\gamma)(1-k)}$. The ring resonator is phase-modulated at modulation frequency $\omega_m$ with modulation index $\beta$.

Assume continuous-wave (CW) laser light is input to the comb generator, and is described by an electric field

$$E_{in}(t) = \hat{E}_{in} e^{j\varphi_o(t)} e^{j\omega_o t}, \tag{4}$$

where $\hat{E}_{in}$, $\omega_o$ and $\varphi_o(t)$ are the input field amplitude, carrier frequency and optical phase noise, respectively. The corresponding output field $E_{out}(t)$ can be expressed as [20]

[1]The subscript "o" stands for "optical" and indicates a variable's association with optical phase noise. The subscript "m" stands for "microwave" and indicates a variable's association with microwave phase noise. The subscripts "0" and "$p_0$" refer to channel numbers. Variables with these subscripts depend on the channel, but are not directly related to optical or microwave phase errors.

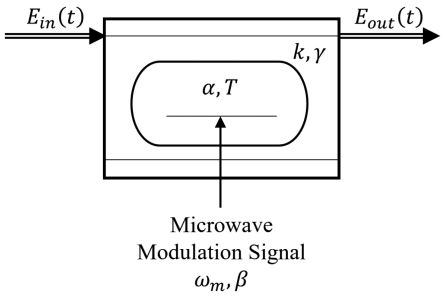


Fig. 9. Resonator-enhanced single-ring electro-optic (SR-EO) frequency comb generator. The input field is coupled into a ring resonator with power transmission $k$ and insertion loss $\gamma$. In the resonator, the optical field experiences round-trip power loss $(1-\alpha)$ and phase modulation at frequency $\omega_m$ with modulation index $\beta$.

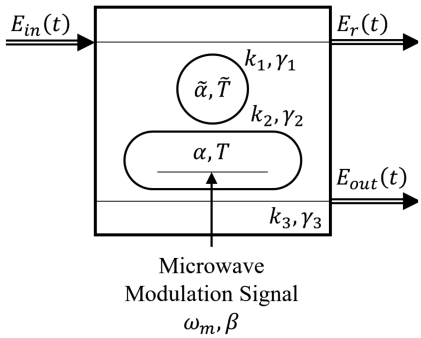


Fig. 10. Dual-ring electro-optic (DR-EO) frequency comb generator. Power first builds up in the small ring and is then coupled to the large resonator, where comb generation occurs. This structure improves comb power conversion efficiency.

$$E_{out}(t) = \sqrt{(1-\gamma)(1-k)}E_{in}(t) - k\sqrt{\frac{1-\gamma}{1-k}}\sum_{n=1}^{\infty} r^n e^{j\beta F_n(\omega_m t)} E_{in}(t-nT) \quad (5)$$

In (5), $F_n(\omega_m t)$ denotes a cascaded modulation function. Assuming the microwave source has a phase noise $\varphi_m(t)$, the cascaded modulation function can be written as

$$F_n(\omega_m t) = \sum_{i=1}^{n} \sin\left[\omega_m t + \varphi_m(t-iT)\right]. \quad (6)$$

In (6), we assume that the modulation frequency $\omega_m$ as well as $\omega_o$ are resonant with the ring's free spectral range (FSR). When optical and microwave phase noises are absent, the Jacobi-Anger expansion can be applied to (5) to obtain the following expression for the output field:

$$E_{out}(t) = \sqrt{(1-\gamma)(1-k)}\hat{E}_{in}e^{j\omega_o t} - k\sqrt{\frac{1-\gamma}{1-k}}\hat{E}_{in}\sum_{p=-\infty}^{\infty}\sum_{n=1}^{\infty} r^n J_p(\beta n)\, e^{j(\omega_o + p\omega_m)t}. \quad (7)$$

The spectrum of $E_{out}(t)$ contains lines at frequencies $\omega_o + p\omega_m$ for integer values of the comb line index $p$.

Fig. 10 shows the DR-EO comb generator, which has an additional small ring with a round-trip time of $\tilde{T}$ and a round-trip loss of $(1-\tilde{\alpha})$. The coupler power transfer coefficients are $k_1$, $k_2$, and $k_3$ and the coupler insertion losses are $\gamma_1$, $\gamma_2$, and $\gamma_3$. The DR-EO comb generator offers more efficient conversion of input power to comb line power, as the small ring facilitates greater power build-up before coupling and comb-generating modulation in the larger ring [14]. We note that in the multi-wavelength analog coherent architecture shown in Fig. 1, the central channel $(p=0)$ uses the field reflected from the DR-EO comb generator input instead of the central line of the output field, as the former has higher power in the design considered below.

The DR-EO comb generator can be analyzed using the steady-state matrix method, a technique that has been used to study free-space Fabry-Pérot resonators [21]. Through the steady-state matrix method, the field of the $p$-th reflected comb line, $E_{r,p}$, and that of the $p$-th output line, $E_{out,p}$, can be computed by solving a system of linear equations. Details on applying the steady-state matrix method to the DR-EO comb generator are presented in [14].

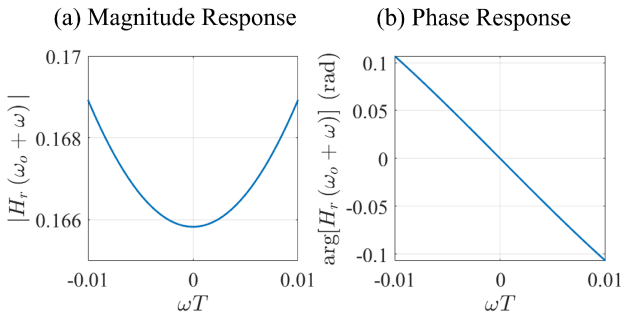


Fig. 11. (a) Magnitude and (b) phase of the transfer function $H_r(\omega)$ describing the mapping of the input seed laser field of the DR-EO comb generator, $E_{in}(t)$, to the field of the 0-th reflected comb line, $E_{r,0}(t)$.

We are interested in how optical and microwave phase noises are affected by the EO comb generator. More specifically, we seek to quantify the optical phase noise appearing on the central channel, which is the $p=0$-th reflected comb line, and the optical phase noise and microwave phase noise appearing on the $p$-th output comb line, where $p \neq 0$. Henceforth, for concreteness, we consider a DR-EO comb generator that has parameter values $\gamma_1 = \gamma_2 = \gamma_3 = 0$, $k_1 = k_2 = k_3 = 0.03$, $\alpha = 0.95$, $\beta = \pi/2$, and $\hat{E}_{in} = 1$. For the small ring, we choose $\tilde{T} = T/16.7$ to concentrate power into the 32 lines nearest to the central line. The power losses of the two resonators are related by $\tilde{\alpha} = \alpha^{\tilde{T}/T}$.

### A. Optical Phase Noise

In order to study how optical phase noise $\varphi_o(t)$ on the seed laser is affected by the DR-EO comb generator, we require a transfer function $H_r(\omega)$ that maps the input field $E_{in}(t)$, at carrier frequency $\omega_o$, to the 0-th line of the DR-EO comb generator reflected field, $E_{r,0}(t)$, also at $\omega_o$. This transfer function can be approximated by solving for $E_{r,0}$ via the steady-state matrix method for input field frequencies close to $\omega_o$.

Fig. 11 shows the computed magnitude and phase responses of the desired transfer function. The magnitude is rather flat and the phase has a near-constant slope in the frequency range near $\omega_o$. These results indicate that $H_r(\omega)$ varies slowly close to $\omega_o$. From Appendix A, an input field $E_{in}(t) = e^{j\varphi_o(t)}e^{j\omega_o t}$ appears on the 0-th reflected comb line in a form $E_{r,0} \propto e^{j\varphi_o(t-\tau_{comb})}e^{j\omega_o t}$, where $\tau_{comb}$ can be computed from the slope of the phase response shown in Fig. 11(b). The delay in the optical phase noise arising from the DR-EO comb generator can be incorporated in the analysis of the central channel OPLL. Referring to the central channel OPLL linearized model in Fig. 8(a), we note that the comb generator delay can be lumped into the loop delay $\tau_o$.

Characterizing the optical phase error between the $p$-th lines of the transmitter and LO combs is also of interest. We can gain insight by studying the SR-EO comb generator. The phase noise-related behavior of the single- and dual-resonator configurations are similar, as the small ring in the DR-EO comb generator is much smaller than the large ring and essentially causes only a small delay in the phase noise processes involved. This is briefly discussed in Appendix B.

Ignoring the microwave phase noise $\varphi_m(t)$ and using the Jacobi-Anger expansion on (5), we can write the $p$-th comb line of the output field as

$$E_{out,p}(t) = -k\sqrt{\frac{1-\gamma}{1-k}} \cdot \times \sum_{n=1}^{\infty} r^n J_p(\beta n)\, e^{j(\omega_o + p\omega_m)t} e^{j\varphi_o(t-nT)}. \quad (8)$$

Let the transmitter and LO comb seed laser optical phase noises be denoted by $\varphi_{o,T}(t)$ and $\varphi_{o,LO}(t)$, respectively. We can determine the optical phase error between the $p$-th transmitter comb output field line $E_{T,p}(t)$ and the $p$-th LO comb output field line $E_{LO,p}(t)$ by evaluating the argument of

$$E^*_{T,p}(t)E_{LO,p}(t) \propto \sum_{m=1}^{\infty}\sum_{n=1}^{\infty} r^{m+n} J_p(\beta m)\, J_p(\beta n) \cdot \times e^{j[-\varphi_{o,T}(t-mT)+\varphi_{o,T}(t-nT)-\varepsilon_o(t-nT)]}. \quad (9)$$

In (9), $\varepsilon_o(t) = \varphi_{o,T}(t) - \varphi_{o,LO}(t)$ is the output phase error of the central channel OPLL (see Fig. 8(a)). Using the central channel OPLL linearized model, the argument of (9) can be numerically computed, and its standard deviation yields the optical phase error. Fig. 12 shows the simulated optical phase error at different comb line indices $p$.

Fig. 12 also shows the phase-error standard deviation of the central channel OPLL, $\sigma_{\varepsilon_o}$ (dashed red). $\sigma_{\varepsilon_o}$ can be calculated using the linearized OPLL model in Fig. 8(a):

$$\sigma^2_{\varepsilon_o} = \frac{\pi\Delta\nu_o}{2\zeta\omega_{n,o}}\Gamma_{\text{PN}}(\omega_{n,o}\tau_o) + \frac{(1+4\zeta^2)\,\omega_{n,o}T_s}{4\zeta}\frac{\eta_c}{2n_{\text{PE}}\gamma_0}\Gamma_{\text{AWGN}}(\omega_{n,o}\tau_o). \quad (10)$$

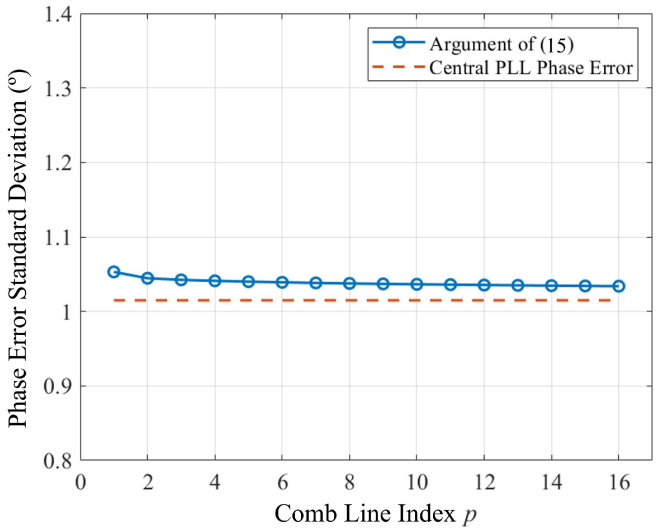


Fig. 12. Standard deviation of the phase error between the transmitter and LO resulting from optical phase noise of the seed lasers for different output comb line indices, $p$. The blue line is obtained by simulating and computing the standard deviation of the argument of (9) for transmitter and LO seed lasers with linewidths of 50 kHz. The dashed red line corresponds to a time-domain simulation of the phase-error standard deviation on the central channel OPLL.

In (10), $\Delta\nu_o$ is the beat linewidth between the transmitter and LO comb seed lasers and $n_{\text{PE}}$ is the number of polarizations used in phase estimation [5]. We assume $n_{\text{PE}} = 2$. $\Gamma_{\text{PN}}(\omega_n\tau)$ and $\Gamma_{\text{AWGN}}(\omega_n\tau)$ are defined by

$$\Gamma_{\text{PN}}(\omega_n\tau) = \frac{2\zeta\omega_n}{\pi}\int_{-\infty}^{\infty} |j\omega + e^{-j\omega\tau}F_o(\omega)|^{-2} d\omega \quad (11)$$

$$\Gamma_{\text{AWGN}}(\omega_n\tau) = \frac{2\zeta}{\pi(1+4\zeta^2)\,\omega_n}\int_{-\infty}^{\infty}\left|\frac{F_o(\omega)}{j\omega + e^{-j\omega\tau}F_o(\omega)}\right|^2 d\omega \quad (12)$$

We observe in Fig. 12 that the optical phase-error standard deviation on the $p$-th output field line is within 3% of that on the central channel. This suggests that, in the presence of only optical phase noise, the phase error performance of non-central channels will be similar to that of the central channel when using only the central-channel OPLL to control the comb seed laser phase noise.

### B. Microwave Phase Noise

The effects of microwave phase noise appear in the SR-EO comb generator output field (5) via the cascaded modulation function $F_n(\omega_m t)$ given by (6). Assuming the coherence time of the microwave phase noise process $\varphi_m(t)$ is much longer than the cavity lifetime of the resonator, we can ignore the delays in the argument of the microwave phase noise and approximate (6) as

$$F_n(\omega_m t) \approx n\sin[\omega_m t + \varphi_m(t)]. \quad (13)$$

The above approximation is extremely accurate, since typical coherence times of the microwave oscillators used for comb

modulation (ms to s) [22] far exceed typical cavity lifetimes of the resonators (ns).

Using (13), the $p$-th output comb line can be written via the Jacobi-Anger expansion as

$$E_{out,p}(t) = -k\sqrt{\frac{1-\gamma}{1-k}} \cdot \times \sum_{n=1}^{\infty} r^n J_p(\beta n)\, e^{j(\omega_o + p\omega_m)t} e^{jp\varphi_m(t)}. \quad (14)$$

From (14), we observe that the microwave phase noise on the $p$-th output comb line is scaled linearly by the comb line index $p$. This introduces the $p_0$ scaling factor in the linearized model of the outer reference OPLL (see Fig. 8(b)). The phase noise characteristics we have derived for the RE-EO comb generator match those derived for non-resonator-enhanced EO comb generators [23].

Let $\varepsilon_m(t)$ denote the difference between the transmitter and LO modulation source microwave phase noises $\varphi_{m,T}(t)$ and $\varphi_{m,LO}(t)$. We can compute the microwave phase error between the $p$-th output field lines of the transmitter and LO combs, $E_{T,p}(t)$ and $E_{LO,p}(t)$, by evaluating the argument of

$$E^*_{T,p}(t)E_{LO,p}(t) \propto e^{jp\varepsilon_m(t)} \sum_{m=1}^{\infty}\sum_{n=1}^{\infty} r^{m+n} J_p(\beta m)\, J_p(\beta n). \quad (15)$$

In the argument of (15), we observe that on the $p$-th output comb line, the microwave phase error $\varepsilon_m(t)$ is scaled by $p$. If the microwave phase error on the outer reference channel is $p_0\varepsilon_m(t)$, choosing the reference channel to be an outermost channel (i.e., $|p_0|$ is a maximal value of $|p|$) will ensure that

$$|p_0|\sigma_{\varepsilon_m} \geq |p|\sigma_{\varepsilon_m}, \quad (16)$$

i.e., the microwave phase-error standard deviation is largest on the outer reference channel.

Combining the optical and microwave phase errors, the phase error on the outer reference channel, as indicated in Fig. 8(b), is $p_0\varepsilon_m(t) + \varepsilon'_o(t)$, where $\varepsilon'_o(t)$ is the phase error on the central channel, $\varepsilon_o(t)$, but modified by the EO comb generation. The optical phase error analysis of the resonator-enhanced electro-optic comb generator shows that $\sigma^2_{\varepsilon'_o} \approx \sigma^2_{\varepsilon_o}$. Denoting the microwave phase-error variance as $\sigma^2_{\varepsilon_m}$, the phase-error variance of the outer reference channel can be estimated as $\sigma^2_{\varepsilon_o} + p_0^2\sigma^2_{\varepsilon_m}$.

Assuming the microwave phase noise can be modeled as a Wiener process with an appropriate choice of beat linewidth $\Delta\nu_m$, the microwave phase-error variance $\sigma^2_{\varepsilon_m}$ can be estimated using an expression similar to (10), choosing a natural frequency $\omega_{n,m}$ and other parameters appropriate to the outer reference channel OPLL. The choice of a beat linewidth $\Delta\nu_m$ providing a conservative estimate of microwave phase noise is discussed in Section IV-A.

## IV. Design Examples

In this section, we describe an exemplary system operating near 1310 nm, which is typical for intra-data center links. The system uses either DP-QPSK or DP-16-QAM modulation at a symbol rate of 56 GBaud, on 17 channels spaced by 100 GHz. The transmitter and LO combs are obtained by taking the central 33 comb lines of a DR-EO comb generator modulated at 50 GHz, using a de-interleaver to keep only the even-indexed lines, corresponding to $p = 0, \pm 2, \ldots, \pm p_0$, with $p_0 = 16$.

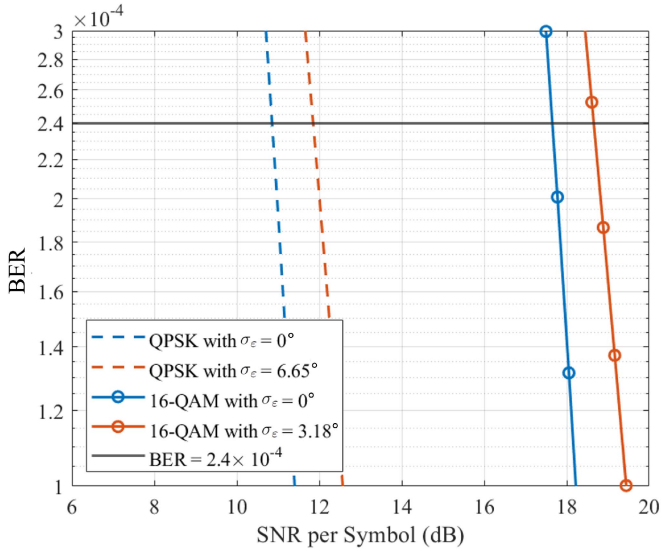


Fig. 13. BER versus SNR per symbol for QPSK (dashed) and 16-QAM (dotted) for different values of the phase-error standard deviation $\sigma_\varepsilon$. For QPSK, the tolerable phase-error standard deviation for a 1-dB SNR penalty at a target BER of $2.4 \times 10^{-4}$ is 6.65°. For 16-QAM, the tolerable phase error is 3.18°.

In this example, we aim for a pre-forward error correction (FEC) bit-error ratio (BER) of $2.4 \times 10^{-4}$, which applies to FEC codes such as RS(544, 514). Achieving this BER requires a SNR per symbol of 17.6 dB for 16-QAM and 10.8 dB for QPSK [1] on an ideal AWGN channel.

### A. Phase Error

The BER of QPSK or 16-QAM including the effects of phase error can be calculated using a numerical integration technique described in [18]. The BER versus SNR per symbol curves at different phase-error standard deviations for both formats are shown in Fig. 13. These curves indicate that achieving a phase error penalty of less than 1 dB requires a phase-error standard deviation below 6.7° for QPSK and below 3.2° for 16-QAM.

The phase-error variance on any channel $p$ is $\sigma^2_{\varepsilon_o} + p^2\sigma^2_{\varepsilon_m}$, as the optical phase error is same across all the channels, while the microwave phase error is scaled by the channel comb line index (see Section III-B). The central channel ($p = 0$) is subject only to optical phase error with a standard deviation $\sigma_{\varepsilon_o}$, which is computed using (10). Figs. 14(a) and 14(b) show $\sigma_{\varepsilon_o}$ as a function of $\omega_{n,o}$, the natural frequency of the central channel OPLL, assuming a beat laser linewidth $\Delta\nu_o = 100$ kHz, for QPSK and 16-QAM, respectively. Focusing on 16-QAM, which poses more stringent phase error requirements than QPSK, we see from Fig. 14(b) that the loop delay $\tau_o$ should not exceed 2 ns to achieve a phase-error standard deviation $\sigma_{\varepsilon_o}$ below the 3.2° needed for a 1-dB phase error penalty.

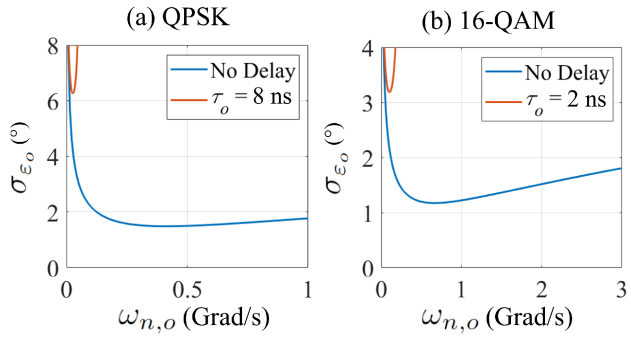


Fig. 14. Phase-error standard deviation $\sigma_{\varepsilon_o}$ versus OPLL natural frequency $\omega_{n,o}$ for the central channel OPLL for various values of the loop delay $\tau_o$ for (a) QPSK and (b) 16-QAM. The beat linewidth is $\Delta\nu_o = 100$ kHz. For a 1-dB SNR penalty at a BER of $2.4 \times 10^{-4}$, the tolerable loop delays are (a) 8 ns for QPSK and (b) 2 ns for 16-QAM.

TABLE I
ESTIMATED DELAYS OF VARIOUS COMPONENTS IN PATH OF CENTRAL CHANNEL OPLL

| Loop Aspect | Components | Delay | Reference |
|---|---|---|---|
| PIC | DP downconverter, optical bandpass filter, SOA* | 100 ps | [24] |
| EIC | Analog phase detector | 100 ps | [25] |
| LF | Loop filter circuits | 100 ps | [25] |
| CG | DR-EO comb generator | 500 ps | N/A |

* The LO comb seed laser is accounted for in subsequent analysis.

Assuming an integrated implementation of the comb-based analog coherent receiver, we provide estimated delays for different components in the central channel OPLL in Table I. The components are categorized as belonging to photonic integrated circuitry (PIC), electronic integrated circuitry (EIC), the loop filter (LF), or the comb generator (CG). The PIC also includes the LO comb seed laser, but we exclude this component from Table I and address its delay requirements separately.

In Table I, the delay associated with the DR-EO comb generator is estimated using the method described in Section III-A. Excluding the delay of the LO comb seed laser, the total round-trip delay through the loop is 800 ps. Hence, the delay associated with frequency modulation (FM) of the LO comb seed laser must not exceed 1.2 ns. Using this value, we can estimate the required LO comb seed laser FM bandwidth. For instance, assuming a first-order laser FM response, the LO laser must have a flat FM response from DC up to a frequency $1/(2\pi \cdot 1.2 \text{ ns}) \approx 150$ MHz.

The LO comb seed laser requirements can be eased by assuming the transmitter comb seed laser linewidth less than 10 kHz, which can be achieved, for example, using an external cavity integrated on silicon [26]. In this case, the LO comb seed laser should have a linewidth less than about 100 kHz and an FM response that is flat up to several hundred megahertz. The multi-electrode DFB laser is a promising candidate to be optimized to achieve these requirements [27].

To study the microwave phase error, we focus on the outermost channels ($|p| = |p_0|$), which have the largest phase-error variance, given by $\sigma^2_{\varepsilon_o} + p_0^2\sigma^2_{\varepsilon_m}$. To make a conservative assessment, we model the combined phase noise of the transmitter and LO microwave oscillators as a Wiener process (corresponding to white frequency noise) described by a beat linewidth $\Delta\nu_m = 1$ kHz. This corresponds to a phase noise of $-98$ dBc/Hz at 1-MHz frequency offset, which is about 9 dB higher than that achieved using low-power monolithic oscillators in this frequency range [28]. Using (10) with a natural frequency $\omega_{n,m}$ and other parameters appropriate to the outer reference channel OPLL, the microwave phase-error standard deviation $p_0\sigma_{\varepsilon_m}$ is found to increase the total phase-error standard deviation by less that 1°. Recall the analysis in Section III-B showing that on all the other channels, the microwave phase-noise standard deviation is smaller than on the outermost channels, i.e., $|p|\sigma_{\varepsilon_m} < |p_0|\sigma_{\varepsilon_m}$.

Since optical phase noise is the dominant source of phase error on all channels, ensuring that phase-error standard deviations do not exceed tolerable values (6.7° for QPSK and 3.2° for 16-QAM) will depend largely on the design and implementation of the central channel OPLL.

TABLE II
LOSS, GAIN AND POWER VALUES FOR EXEMPLARY COMB-BASED SYSTEM

| | |
|---|---|
| Tx output coupling, de-interleaving, and flattening loss ($\eta_1$, $\eta_{1,LO}$) | 10 dB |
| Tx (de-)multiplexing, and DP-IQ modulation loss ($\eta_2$) | 10 dB |
| LO de-multiplexing loss ($\eta_{2,LO}$) | 10 dB |
| Fiber span loss ($\eta_3$) | 6.3 dB |
| Rx de-multiplexing, polarization controller, and downconversion loss ($\eta_4$) | 10 dB |
| Booster amplifier 1 gain ($G_1$) | 30 dB |
| LO booster amplifier gain ($G_{LO}$) | 22 dB |
| Booster amplifier noise figure ($F_{n,1}$, $F_{n,LO}$) | 7 dB |
| Tx comb input power ($P_{in,T}$) | 16 dBm |
| LO comb input power ($P_{in,LO}$) | 24 dBm |

## B. Dispersion

Using Monte Carlo simulations, we have determined the dispersion values resulting in penalties not exceeding 1 dB for QPSK or 16-QAM at a symbol rate of 56 Gbaud. These simulations assumed 5-th order Bessel transmitter and receiver with bandwidths equal to 0.7 times the symbol rate. For a target BER of $2.4 \times 10^{-4}$, the tolerable dispersion values for a 1-dB SNR penalty are about 25 ps/nm for QPSK and 12 ps/nm for 16-QAM. Assuming standard single-mode fiber and 17 channels with 100-GHz spacing centered at 1310 nm, these correspond to dispersion-limited reaches of more than 25 km for 16-QAM and more than 50 km for QPSK, significantly exceeding the longest intra-data center links [29].

## C. Signal-to-Noise Ratio

Other noise sources in the comb-based link are analyzed in Appendix C. Expressions for the variances of the different noises can be used to compute the SNR per symbol for each wavelength channel in the system. Losses in the system are labelled $\eta_i$ and gains by $G_i$ in Fig. 1. The loss, gain and power values assumed in this design example are given in Table II.

Accounting for a 0.5-dB penalty from the marker tone-based polarization and phase offset control (Section II-B), a 1-dB penalty from phase error, a 1-dB penalty from chromatic dispersion and 1 dB for other implementation penalties, we need and SNR of 21.1 dB for 16-QAM. Using the values from Table II, photodiode responsivity, $R = 1$ A/W, and the noise variance expressions in Appendix C, we find the channel with the lowest power has an SNR per symbol of about 22.0 dB, exceeding the 21.1 dB required for 16-QAM.

The parameter values in Table II are chosen conservatively to accommodate the losses in integrated photonic realizations of the transmitter and receiver. The total transmitter output power is less than 20 dBm to ensure eye safety [30]. The total output power at each SOA does not exceed 24 dBm [31]. The input optical powers to the transmitter and LO comb generators are 16 dBm and 24 dBm, respectively, well below the 33-dBm damage threshold for thin-film lithium niobate waveguides [32]. The LO comb input power of 24 dBm can be achieved, for example, by using an LO comb seed laser with 14-dBm output power, followed by an integrated SOA with 10-dB gain.

The LO comb generator input power of 24 dBm may be sufficient to induce four-wave mixing (FWM) and Raman scattering in the comb generator [33] and FWM in the SOA at the comb generator output. Frequency components generated by FWM coincide with the EO-generated comb lines. The phase noises on the FWM-generated lines depend on the optical phase noise $\varphi_o(t)$, microwave phase noise $\varphi_m(t)$ and comb line index $p$ in the same way as the phase noises on the EO-generated lines. Raman gain does not itself affect the comb phase noise. Thus, the phase noise models developed in Section III should remain valid.

Our design examples have emphasized 16-QAM, as it is more difficult to realize than QPSK, and studying it helps illuminate the challenges and solutions for achieving high SNR and low phase error. QPSK, while providing only half the bit rate of 16-QAM, has several properties that ease the realization of comb-based links. QPSK can operate at a lower SNR per symbol. QPSK can tolerate a higher phase-error standard deviation, so wider laser linewidths and longer loop delays can be tolerated. QPSK can employ simpler phase detectors, such as the Costas phase detector or the multiplier-free phase detector described in [5]. Finally, a DP-QPSK signal is binary in each dimension, making this format very tolerant to bandwidth limitations in transmitter and receiver components [5]. Integrated OPLL-based coherent receivers using QPSK have been demonstrated [13], [34].

## V. Conclusion

We have studied a comb-based analog coherent receiver for WDM optical data center links that uses DR-EO comb generators as transmitter and LO sources. By analyzing the comb generator phase noise properties, we have shown that CR on all wavelength channels can be achieved using two OPLLs. We also showed that polarization de-multiplexing and removal of constant phase offsets can be performed using cascaded optical phase shifters controlled by low-speed marker tones. This scheme results in a 0.5-dB SNR penalty at a $2.4 \times 10^{-4}$ target BER for 16-QAM. The proposed design was considered for both DP-QPSK and DP-16-QAM modulation formats operating at 56 Gbaud. DP-16-QAM poses more stringent phase-error requirements, and accommodating this format will require an LO seed laser with linewidth of about 100 kHz and an FM response that is flat from DC to several hundred MHz to maintain a phase-error penalty below 1 dB. For DP-16-QAM, dispersion should not exceed 12 ps/nm for a penalty of 1 dB.

## Appendix A
## Comb Transfer Function

The passband channel from the comb generator seed laser input to the 0-th reflected line can be denoted as $H_r(\omega)$, and has the form

$$H_r(\omega) = |H_r(\omega)|e^{j\arg[H_r(\omega)]}. \tag{17}$$

We consider an input signal $E_{in}(t)$ of the form

$$E_{in}(t) = u(t)e^{j\omega_o t}, \tag{18}$$

where $u(t)$ is an envelope modulating the carrier at frequency $\omega_o$. If $H_r(\omega)$ varies slowly as a function of $\omega$ near frequency $\omega_o$, we can make the approximation

$$H_r(\omega_o + \omega) \approx H_r(\omega_o)\, e^{-j\omega\tau_{comb}}. \tag{19}$$

(19) is obtained using Taylor series approximations on both $|H_r(\omega_o + \omega)|$ and $\arg[H_r(\omega_o + \omega)]$, while $\tau_{comb}$ is computed from the phase response of $H_r(\omega)$:

$$\tau_{comb} \equiv -\left.\frac{d\arg\left[H_r(\omega)\right]}{d\omega}\right|_{\omega=\omega_o} \tag{20}$$

Letting $h_r(t)$ denote the impulse response of the passband channel $H_r(\omega)$, the 0-th reflected line $E_{r,0}(t)$ can be expressed as a convolution:

$$\begin{aligned} E_{r,0}(t) &= [u(t) * h_r(t)]\, e^{j\omega_o t} \\ &\approx H_r(\omega_o)\, F^{-1}\left\{U(\omega)\, e^{-j\omega\tau_{comb}}\right\} e^{j\omega_o t} \\ &= H_r(\omega_o)\, u(t - \tau_{comb})\, e^{j\omega_o t}. \end{aligned} \tag{21}$$

In (21), $F^{-1}\{\cdot\}$ denotes an inverse Fourier transform. The effect of the comb generator on the envelope function $u(t)$ can be expressed as a delay.

## Appendix B
## Equivalence of SR- and DR-EO Comb Generators

To study the DR-EO comb generator output, we focus on field copies that have travelled through the small ring $\widetilde{n}$ times and then the large ring $n$ times before exiting through the output port. We do not consider field copies that return to the small ring after entering the large ring. We are able to make this assumption because the coupling probability between the small and large ring is designed to be low.

For the contributions to the output field $E_{out}(t)$ that we are interested in, we can show that

$$E_{out}(t) \propto \sum_{\widetilde{n}=0}^{\infty}\sum_{n=0}^{\infty} e^{j\omega_o \widetilde{n}\widetilde{T}}\widetilde{r}^{\widetilde{n}} e^{j\beta n \sin(\omega_m t)} r^n \cdot \times E_{in}\left(t - \frac{\widetilde{T}}{2} - \frac{T}{2} - nT\right). \tag{22}$$

Considering an input seed laser field with optical phase noise $\varphi_o(t)$ we have $E_{in}(t) = e^{j\omega_o t}e^{j\varphi_o(t)}$ and (22) becomes

$$E_{out}(t) \propto e^{j\omega_o t}\cdot\left(\sum_{\widetilde{n}=0}^{\infty} e^{j\omega_o\widetilde{n}\widetilde{T}}\widetilde{r}^{\widetilde{n}}\right)\cdot \times\left(\sum_{n=0}^{\infty} r^n e^{j\omega_o nT} e^{j\beta n\sin(\omega_m t)} e^{j\varphi_o\left(t-\frac{\widetilde{T}}{2}-\frac{T}{2}-nT\right)}\right) \tag{23}$$

Applying the Jacobi-Anger expansion, the $p$-th output comb line field can be written as

$$E_{out,p}(t) \propto \sum_{n=0}^{\infty} r^n J_p(\beta n)\, e^{j(\omega_o + p\omega_m)t} e^{j\varphi_o\left(t-\frac{\widetilde{T}}{2}-\frac{T}{2}-nT\right)}. \tag{24}$$

(24) has a form similar to (8), except for additional delay in the $\varphi_o(t)$ term. This constant delay is not expected to affect the time-dependent optical phase noise on the $p$-th output comb line. We therefore model phase errors considering SR-EO comb generators to simplify and clarify the analysis.

## Appendix C
## Noise Sources

We study the various noise sources of the comb-based link in this section. Noise in coherent systems typically includes shot noise, thermal noise, and LO-signal spontaneous beat noise [1]. Because using a frequency comb source for the LO requires operations such as amplification, flattening, and de-interleaving, a noise source, perhaps unique to comb-based receivers, arises when amplified spontaneous emission (ASE) added to the LO beats with the signal. We may call this the *signal-LO spontaneous beat noise*.

Fig. 15 shows the possible input components to the 90°-hybrid of the downconverter in one polarization for one system channel.

At the output of a single balanced photodiode pair, the variances of the thermal, shot, and LO-signal spontaneous beat noise for a receiver electrical filter of bandwidth $\Delta f$ and for wavelength de-multiplexers of bandwidth $\Delta\nu_s$ and $\Delta\nu_{LO}$ for the signal and LO, respectively, are [1]

$$\sigma^2_{thermal} = N_0\Delta f \tag{25}$$

$$\sigma^2_{shot} = qR(\eta_4 P_s + \eta_{2,LO}P_{LO} + \eta_4 S_{sp,s}\Delta\nu + \eta_{2,LO}S_{sp,LO}\Delta\nu_{LO})\Delta f \tag{26}$$

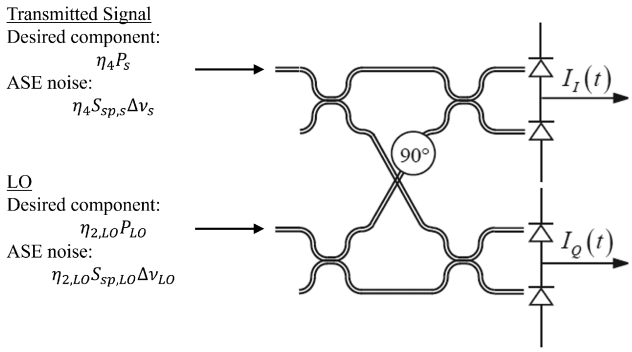


Fig. 15. Various signal and noise components entering the 90° hybrid in the coherent detection downconverter. $S_{sp,s}$ and $S_{sp,LO}$ are the power spectral densities (PSDs) per polarization of the spontaneous emission noises on the signal and LO, respectively.

$$\sigma^2_{LO-sig.spont} = R^2\eta_{2,LO}P_{LO}\eta_4 S_{sp,s}\min\left(\Delta f, \frac{\Delta\nu_s}{2}\right) \tag{27}$$

In the equations above, $S_{sp,s}$ and $S_{sp,LO}$ are the one-sided PSDs per polarization of the ASE noise on the signal and LO, respectively. $P_s$ and $P_{LO}$ are the average signal and LO powers per channel per polarization at the locations specified in Fig. 1, respectively. $N_0$ is the one-sided thermal noise PSD and $R$ is the photodiode responsivity. Signal-LO spontaneous beat noise is similar to LO-signal spontaneous beat noise in that they both involve ASE beating with a narrow-bandwidth signal. Instead of being caused by ASE carried with the data-bearing signal beating with the continuous-wave LO carrier, signal-LO spontaneous beat noise arises from ASE carried with the LO beating with the data-bearing signal. We notice a symmetry between the variance of the LO-signal spontaneous beat noise in (27) and the variance of the signal-LO spontaneous beat noise, which is given by

$$\sigma^2_{sig.-LOspont} = R^2\eta_4 P_s\eta_{2,LO}S_{sp,LO}\min\left(\Delta f, \frac{\Delta\nu_{LO}}{2}\right) \tag{28}$$

Of the noise sources identified, LO-signal spontaneous beat noise and thermal noise are signal-independent. Signal-LO spontaneous beat noise is signal-dependent. Shot noise has both signal-dependent and signal-independent components. In the 16-QAM design example in Section IV, a corner constellation point has a total noise variance less than 5% larger than that on an inner point, indicating that the noise is dominated by signal-independent components.

## Acknowledgment

The authors are grateful for helpful discussions with Prof. L. A. Coldren, E. S. Chou, Y. Hu, J. K. Perin, A. Shastri, and M. Yu.

## References

[1] E. Ip, A. P. T. Lau, D. J. F. Barros, and J. M. Kahn, "Coherent detection in optical fiber systems," *Opt. Exp.*, vol. 16, no. 2, pp. 753–791, 2008.
[2] G. P. Agrawal, *Fiber-Optic Communication Systems*, 3rd ed. Hoboken, NJ, USA: Wiley, 2002.

[3] B. Buscaino, B. D. Taylor, and J. M. Kahn, "Multi-Tb/s-per-fiber coherent co-packaged optical interfaces for data center switches," *J. Lightw. Technol.*, vol. 37, no. 13, pp. 3401–3412, 2019.
[4] N. Nambath, R. K. Raveendranath, D. Banerjee, A. Sharma, A. Sankar, and S. Gupta, "Analog domain signal processing-based low-power 100-Gb/s DP-QPSK receiver," *J. Lightw. Technol.*, vol. 33, no. 15, pp. 3189–3197, 2015.
[5] J. K. Perin, A. Shastri, and J. M. Kahn, "Design of low-power DSP-free coherent receivers for data center links," *J. Lightw. Technol.*, vol. 35, no. 21, pp. 4650–4662, 2017.
[6] M. Morsy-Osman et al., "DSP-free 'coherent-lite' transceiver for next generation single wavelength optical intra-datacenter interconnects," *Opt. Exp.*, vol. 26, no. 7, pp. 8890–8903, 2018.
[7] N. Nambath et al., "All-analog adaptive equalizer for coherent data center interconnects," *J. Lightw. Technol.*, vol. 38, no. 21, pp. 5867–5874, Nov. 2020.
[8] D. Kong et al., "Intra-datacenter interconnects with a serialized silicon optical frequency comb modulator," *J. Lightw. Technol.*, vol. 38, no. 17, pp. 4677–4682, Sep. 2020.
[9] L. Lundberg et al., "Phase-coherent lightwave communications with frequency combs," *Nature Commun.*, vol. 11, 2020, Art. no. 201.
[10] L. Lundberg et al., "Frequency comb-based WDM transmission systems enabling joint signal processing," *Appl. Sci.*, vol. 8, 2018, Art. no. 718.
[11] A. C. Bordonalli, M. J. Fice, and A. J. Seeds, "Optical injection locking to optical frequency combs for superchannel coherent detection," *Opt. Exp.*, vol. 23, no. 2, pp. 1547–1557, 2015.
[12] M. Mazur, A. Lorences-Riesgo, J. Schröder, P. A. Andrekson, and M. Karlsson, "10 tb/s PM-64QAM self-homodyne comb-based superchannel transmission with 4% shared pilot tone overhead," *J. Lightw. Technol.*, vol. 36, no. 16, pp. 3176–3184, Aug. 2018.
[13] T. Hirokawa et al., "Analog coherent detection for energy efficient intra-data center links at 200 Gbps per wavelength," *J. Lightw. Technol.*, vol. 39, no. 2, pp. 520–531, 2021.
[14] B. Buscaino, M. Zhang, M. Loncar, and J. M. Kahn, "Design of efficient resonator-enhanced electro-optic frequency comb generators," *J. Lightw. Technol.*, vol. 38, no. 6, pp. 1400–1413, Jan. 2021.
[15] H. Bulow et al., "Measurement of the maximum speed of PMD fluctuation in installed field fiber," in *Proc. Tech. Dig. Opt. Fiber Conf., Int. Conf. Integr. Opt. Opt. Fiber Commun.*, 1999, pp. 83–85.
[16] H. Zhou et al., "Compact, submilliwatt, $2 \times 2$ silicon thermo-optic switch based on photonic crystal nanobeam cavities," *Photon. Res.*, vol. 5, no. 2, pp. 108–112, 2017.
[17] J. R. Barry and J. M. Kahn, "Carrier synchronization for homodyne and heterodyne detection of optical quadriphase-shift keying," *J. Lightw. Technol.*, vol. 10, no. 12, pp. 1939–1951, 1992.
[18] E. Ip and J. M. Kahn, "Carrier synchronization for 3- and 4-bit-per-Symbol optical transmission," *J. Lightw. Technol.*, vol. 23, no. 12, pp. 4110–4124, 2005.
[19] A. Ishizawa et al., "Phase-noise characteristics of a 25-GHz-spaced optical frequency comb based on a phase- and intensity-modulated laser," *Opt. Exp.*, vol. 21, no. 24, pp. 29186–29194, 2013.
[20] K. P. Ho and J. M. Kahn, "Optical frequency comb generator using phase modulation in amplified circulating loop," *IEEE Photon. Technol. Lett.*, vol. 5, no. 6, pp. 721–725, Jun. 1993.
[21] R. P. Kovacich, U. Sterr, and H. R. Telle, "Short-pulse properties of optical frequency comb generators," *Appl. Opt.*, vol. 39, no. 24, pp. 4372–4376, 2000.
[22] J. Craninckx and M. Steyaert, "Low-noise voltage-controlled oscillators using enhanced LC-tanks," *IEEE Trans. Circuits Syst. - II: Analog Digit. Signal Process.*, vol. 42, no. 12, pp. 794–804, Dec. 1995.
[23] L. Lundberg, M. Mazur, A. Fulop, V. Torres-Company, M. Karlsson, and P. A. Andrekson, "Phase correlation between lines of electro-optical frequency combs," in *Proc. Conf. Lasers Electro- Opt.*, 2018, pp. 1–2.
[24] M. Lu et al., "An integrated 40 Gbit/s optical costas receiver," *J. Lightw. Technol.*, vol. 31, no. 13, pp. 2244–2253, Jul. 2013.
[25] H. Park et al., "40 Gbit/s coherent optical receiver using a costas loop," *Opt. Exp.*, vol. 20, no. 26, pp. B197–B203, 2012.
[26] D. Huang et al., "High-power sub-kHz linewidth lasers fully integrated on silicon," *Optica*, vol. 6, no. 6, pp. 745–752, 2019.
[27] K. Dridi, R. Maldonado-Basilio, A. Benhsaien, X. Zhang, and T. J. Hall, "Low-threshold and narrow linewidth two-electrode MQW laterally coupled distributed feedback lasers at 1550 nm," in *Proc. 38th Eur. Conf. Exhib. Opt. Commun.*, 2012, pp. 1–3.
[28] H. Li and H.-M. Rein, "Millimeter-wave VCOs with wide tuning range and low phase noise, fully integrated in a SiGe bipolar production technology," *IEEE J. Solid-State Circuits*, vol. 38, no. 2, pp. 184–191, Feb. 2003.
[29] J. K. Perin, A. Shastri, and J. M. Kahn, "Data center links beyond 100 Gbit/s per wavelength," *Opt. Fiber Technol.*, vol. 44, pp. 69–85, 2018.
[30] B. Buscaino, E. Chen, J. W. Stewart, T. Pham, and J. M. Kahn, "External vs. integrated light sources for intra-data center co-packaged optical interfaces," *J. Lightw. Technol.*, vol. 39, no. 7, pp. 1984–1996, Apr. 2021.
[31] S. Liu et al., "High efficiency, high gain and high saturation output power quantum dot SOAs grown on Si and applications," in *Proc. Opt. Fiber Commun. Conf. Exhib.*, 2020, pp. 1–3.
[32] C. Wang, M. Zhang, M. Yu, R. Zhu, H. Hu, and M. Loncar, "Monolithic lithium niobate photonic circuits for kerr frequency comb generation and modulation," *Nature Commun.*, vol. 10, no. 1, 2019, Art. no. 978.
[33] Y. Hu et al., "High-efficiency and broadband electro-optic frequency combs using coupled lithium-niobate microresonators," in *Proc. Conf. Lasers Electro-Opt.*, May 2021.
[34] P. J. Skahan, S. Gundavarapu, K. N. Nguyen, D. M. Baney, and D. J. Blumenthal, "Monolithically integrated dual-channel coherent receiver with widely tunable local oscillator for 100 Gbps dual-polarization quadrature phase shift keying applications," *Opt. Lett.*, vol. 40, no. 18, pp. 4313–4316, 2015.

**Elizabeth Chen** (Student Member, IEEE) received the B.A.Sc. degree in engineering science from the University of Toronto, Toronto, ON, Canada, in 2019, and the M.S. degree in electrical engineering in 2021 from Stanford University, Stanford, CA, USA,where she is currently working toward the Ph.D. degree in electrical engineering. Her research interests include optical communications, optical frequency combs, and coherent data center links.

**Brandon Buscaino** (Member, IEEE) received the B.S. degree in physics and the M.S. and Ph.D. degrees in electrical engineering from Stanford University, Stanford, CA, USA, in 2015, 2016, and 2020 respectively. He is currently with Ciena Corporation as a Research Scientist. His research interests include coherent optical fiber communications, electro-optic frequency combs, intra-data center link design, and co-packaged optics.

**Joseph M. Kahn** (Fellow, IEEE) received the A.B., M.A., and Ph.D. degrees in physics from the University of California, Berkeley, Berkeley, CA, USA, in 1981, 1983, and 1986, respectively. In 1987–1990, he was with AT&T Bell Laboratories. In 1989, he demonstrated the first successful synchronous (coherent) detection using semiconductor lasers, achieving record receiver sensitivity. In 1990–2003, he was on the Electrical Engineering and Computer Sciences Faculty at Berkeley. He demonstrated coherent detection of QPSK in 1992. In 1999, D.-S. Shiu and Kahn published the first work on probabilistic shaping for optical communications. In the 1990 s and early 2000 s, Kahn and collaborators performed seminal work on indoor and outdoor free-space optical communications and multi-input multi-output wireless communications. In 2000, Kahn and K.-P. Ho founded StrataLight Communications, whose 40 Gb/s-per-wavelength long-haul fiber transmission systems were deployed widely by AT&T, Deutsche Telekom, and other carriers. In 2002, Ho and Kahn applied to patent the first electronic compensation of fiber Kerr nonlinearity. StrataLight was acquired by Opnext in 2009. In 2003, Kahn became a Professor of electrical engineering with the E. L. Ginzton Laboratory, Stanford University, Stanford, CA, USA. Kahn and collaborators have extensively studied rate-adaptive coding and modulation, and also digital signal processing for mitigating linear and nonlinear impairments in coherent systems. In 2008, E. Ip and Kahn (and G. Li independently) invented simplified digital backpropagation for compensating fiber Kerr nonlinearity and dispersion. Since 2004, Kahn and collaborators have studied propagation, modal statistics, spatial multiplexing and imaging in multi-mode fibers, elucidating principal modes and demonstrating transmission beyond the traditional bandwidth-distance limit in 2005, deriving the statistics of coupled modal group delays and gains in 2011, and deriving resolution limits for imaging in 2013. His research interests include optical frequency comb generators, coherent data center links, rate-adaptive access networks, fiber Kerr nonlinearity mitigation, ultra-long-haul submarine links, and optimal free-space transmission through atmospheric turbulence. Kahn was the recipient of the National Science Foundation Presidential Young Investigator Award in 1991. In 2000, he became a Fellow of the IEEE.